Sound transmission loss characteristics of sandwich panel constructions

J. A. Moore[a] and R. H. Lyon
Department of Mechanical Engineering, Masschusetts Institute of Technology, Cambridge, Massachusetts 02139

(Received 10 August 1989; revised 18 June 1990; accepted 5 September 1990)

The sound transmission loss (TL) characteristics of panel constructions with thin face sheets and a thicker, lighter core are investigated. Analytical models of TL are developed for constructions with isotropic and orthotropic core materials. The occurrence of acoustic coincidence is described for symmetric and antisymmetric modes of propagation in the panel. Symmetric propagation involves thickness deformation of the core, while antisymmetric propagation involves a bending deformation of the panel without thickness deformation. For symmetric modes, coincidence occurs near the conventional double wall resonance frequency characterized by the stiffness of the core and the mass of the face sheets, and also at higher frequencies associated with bending wave propagation in the face sheets. Antisymmetric modes account for shear deformation in the core, which results in a softening of the bending rigidity of the panel at higher frequencies. For orthotropic core materials, the acoustic behavior is dependent on the direction of propagation over the surface of the panel. Measured TL results for representative panels show good agreement with predictions. Finally, a procedure for obtaining improved TL performance is described, which involves shifting the double wall resonance to below the frequency band of interest, and limiting the shear stiffness of the core to shift the onset of bending wave coincidence to higher frequencies. Greater than mass law TL, similar to that of conventional double wall constructions, can be achieved over a significant frequency band in the audio range. The mechanical integrity of the panel is provided by the shear stiffness of the core.

PACS numbers: 43.55.Rg

LIST OF SYMBOLS

A_+, A_-	amplitudes of dilatational wave potential function
B_+, B_-	amplitudes of shear wave potential function
c	wave speed in sandwich panel
c_d, c_s	dilatational/shear wave speed in elastic medium
c_0	sound speed in air
c_t	trace acoustic wave speed on panel surface
D	bending rigidity of face sheet
E_{ij}	elastic stiffness of orthotropic core material
E_{11}^{fs}	elastic stiffness of face sheet: $E/(1-\nu^2)$
G	shear modulus of isotropic core material
h_x, h_y	dimensions of test panel
i	$\sqrt{-1}$
I	acoustic intensity
k	wave number, subscript corresponds to motion type or direction
L	thickness of the core material
m	mass per unit surface area of face sheet
P_a, P_s	antisymmetric/symmetric acoustic pressure amplitudes
P_1, P_2	acoustic pressures on top/bottom panel surfaces
$q, \dot{q}$	generalized displacement/velocity
t	face sheet thickness
u, v, w	displacements in x, y, z directions, subscript indicates panel component
W	strain energy density
Z_a, Z_s	impedances for antisymmetric/symmetric panel motions
$\alpha, \beta, \gamma, \zeta$	displacement amplitudes
ϵ_i, γ_{ij}	normal/shear strains
η	damping loss factor
θ, ϕ	polar/azimuthal angles
Φ, ψ	dilatational/shear wave potential functions
λ	wavelength
μ, λ	Lame's constants for core material
ν	Poisson's ratio of face sheet
σ_i, τ_{ij}	normal/shear stresses
$\tau(\theta, \phi)$	transmission coefficient
ω	radian frequency

INTRODUCTION

The sound-insulating characteristics of walls, floors, and ceilings in buildings and of the walls of machinery enclo-

[a] Present address: Department of Mechanical Engineering, University of Lowell, One University Avenue, Lowell, Massachusetts 01854.

 0001-4966/91/020777-15$00.80

sures are an important aspect of their design. At present, studded wall constructions are available that may provide sufficient attenuation of sound across the wall. Such constructions require on-site fabrication. Premade partitions with adequate TL are available but must be manufactured to exact dimensions. Sandwich panel constructions, fabricated under controlled factory conditions, that can be cut to size on-site, offer advantages over conventional approaches if the TL characteristics are adequate for the application.

Over the years, a great deal of research has been carried out in identifying the TL characteristics of different panel constructions. Unique approaches to achieving high TL within mass limitations include a design developed by Watters and Kurtze,[1] the "shear wall," and the "coincidence wall" developed by Warnaka[2] and Holmer.[3] These designs are based on an understanding of coincidence effects in the interaction of the incident sound field with the vibration response of the panel. Coincidence involves a matching of wave speeds between the incident sound field as it propagates across the surface of the panel and the wave speed of vibratory motion within the panel. It results in a reduction in acoustic TL performance of the panel. The design procedure for the shear wall is to avoid coincidence in the frequency band of interest. The coincidence wall seeks to lessen the adverse effects of coincidence through damping control of panel response.

Bending deformation in a sandwich panel construction was characterized by Ross *et al.*[4] Their descriptions of bending rigidity were utilized by Holmer in the development of the coincidence wall design. Manning[5] studied procedures for optimizing the performance of the coincidence wall and developed expressions for the effective damping in panels with 3, 4, and 5 layers.

The first effort at describing the effects of the thickness deformation on panel TL is attributable to Ford *et al.*[6] Panel dynamics were characterized using a variational approach with assumed displacement fields for the face sheets and core of a three layer panel configuration. The face sheets and core consisted of homogeneous, isotropic materials.

Subsequent investigators, Smolenski and Krokosky,[7] and Dym and Lang,[8] have applied essentially the same approach in studying the effects of core compliance on panel TL. An additional panel motion, referred to in the present discussion as the symmetric mode, occurs in which the face sheet motions are out of phase. Thickness deformation of the core is important in determining the frequency location of the double wall resonance of the panel and the resulting reduction in TL. Ford *et al.*[6] and Smolenski and Krokosky[7] computed wave speeds for symmetric panel motions that are used to identify regions where coincidence occurs.

The approach of Ford *et al.*[6] was extended by Moore[9] and in the present paper for symmetric panel configurations with orthotropic as well as isotropic core materials. Dym and Lang[10] further extended the analysis approach for panels with differing face sheets in relaxing the symmetric panel configuration restriction. Parametric studies led them to the apparent conclusion that face sheet asymmetries degrade acoustic TL performance over that provided by symmetric configurations.

Makris *et al.*[11] utilized the analysis for symmetric panel configurations to develop an optimization procedure where the figure of merit was a weighted average of transmission coefficient values in the frequency range from 1–4 kHz. Functional relationships were developed between the average TL and core thickness and density values with constraints on the total surface mass of the panel.

The work reported herein extends the earlier analysis approach of Ford *et al.*[6] to apply for panel configurations with orthotropic cores, including materials such as resin impregnated paper honeycomb. In addition, for isotropic core materials, such as closed- or open-cell foams, an analysis is developed that describes, in complete generality, the propagation of shear and dilatational waves within the core, and their interaction with the face sheets in transmitting sound through the panel.

A novel panel design approach has been developed and patented for sandwich panels with greater than mass law TL.

Section I describes the development of panel vibration models for constructions with both isotropic and orthotropic core materials. Both the symmetric, i.e., thickness deformation, and antisymmetric, i.e., bending deformation, modes of panel vibration are considered. Transmission loss performance is evaluated and explained for test panels with both isotropic and orthotropic cores.

In Sec. II, an alternative design approach to the shear and coincidence wall designs is presented. The design is referred to as the "mode canceling panel for high TL."[12] It offers greater than mass law TL performance similar to carefully designed conventional dry wall constructions in a sandwich construction that also provides mechanical load bearing capacity. Through judicious choice of bulk and shear stiffness moduli for the core, the double wall resonance is shifted to below the frequency band of interest and coincidence, due to panel bending, is delayed to high frequency. A test panel was fabricated and experimentally evaluated in demonstrating the design approach.

I. TL MODELS

Only symmetric panel configurations are considered; the face sheets are identical and the core material is homogeneous. The dynamics of the panel are then readily described in terms of symmetric and antisymmetric panel impedances, as illustrated in Fig. 1. The actual pressure fields acting on the top and bottom face sheets of the panel are decomposed into symmetric and antisymmetric pressure terms as follows:

$$P_s = (P_1 + P_2)/2, \quad P_a = (P_1 - P_2)/2. \tag{1}$$

Transverse and in-plane motions of the face sheets are also decomposed into symmetric and antisymmetric terms as follows:

$$w_s = (w_1 - w_2)/2, \quad w_a = (w_1 + w_2)/2, \tag{2}$$
$$u_s = (u_1 + u_2)/2, \quad u_a = (u_1 - u_2)/2.$$

For acoustic plane-wave incidence on a panel of infinite extent, the pressure fields and velocity response of the panel are functions of frequency, the angle of incidence with respect to the normal to the panel, and, for orthotropic core

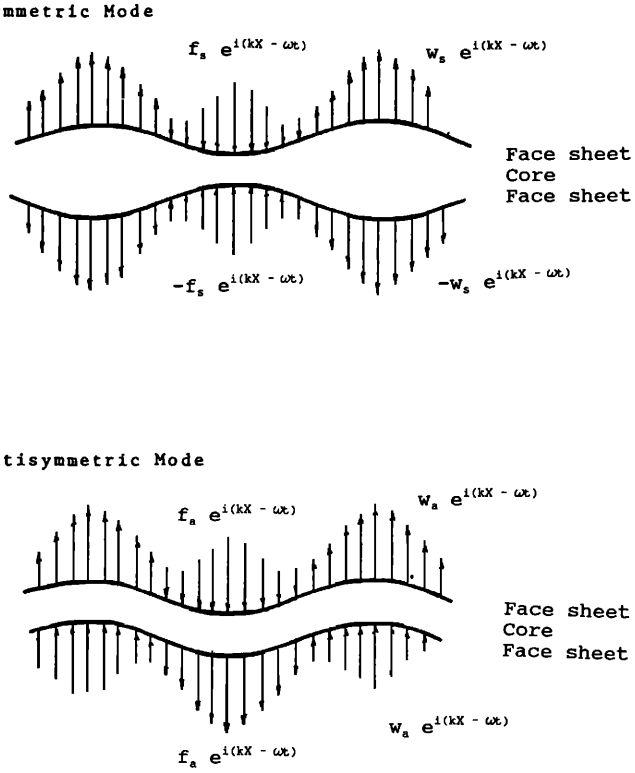

FIG. 1. Symmetric and antisymmetric motions in a sandwich panel.

configurations, the direction of propagation over the surface of the panel. The amplitude ratio of the pressure at the panel surface to the panel velocity defines panel impedances for both symmetric and antisymmetric motions:

$$\begin{Bmatrix} -P_s \\ -P_a \end{Bmatrix} = \begin{bmatrix} Z_s & 0 \\ 0 & Z_a \end{bmatrix} \begin{Bmatrix} w_s \\ w_a \end{Bmatrix}. \tag{3}$$

The negative sign accounts for a difference in sign convention for force per unit area and acoustic pressure. For symmetric panel configurations, symmetric and antisymmetric motions are uncoupled.

The acoustic transmission coefficient is defined as the ratio of the transmitted to incident acoustic intensities. It is evaluated in terms of the symmetric and antisymmetric panel impedances, and the characteristic impedance of air:

$$\tau(\theta,\phi) = |I_{\text{trans}}/I_{\text{inc}}|^2 = \left| \frac{(\rho_0 c_0/\cos\theta)(Z_s - Z_a)}{(Z_s + \rho_0 c_0/\cos\theta)(Z_a + \rho_0 c_0/\cos\theta)} \right|^2. \tag{4}$$

This expression provides insight in understanding the TL behavior of sandwich panel configurations. If, for particular conditions of frequency and orientation of the incident plane wave $Z_a = 0$, then Eq. (4) yields the following:

$$\tau(\theta,\phi) = |Z_s/(Z_s + \rho_0 c_0/\cos\theta)|^2$$

and

$$\tau(\theta,\phi) \cong 1, \tag{5}$$

where it is assumed for lightly fluid-loaded panels in air that $Z_s > \rho_0 c_0/\cos\theta$. The same behavior occurs if $Z_s = 0$.

This condition, characterized by a peak in the transmission through the panel, is referred to as coincidence. For a panel excited by an acoustic wave, as in Eq. (4), a zero value for either Z_a or Z_s occurs when the wave speed of the trace acoustic wave propagating across the surface of the panel matches the wave speed for motion within the panel. This matching condition depends not only on frequency but the trace wave number of the acoustic excitation on the panel surface.

Panel damping adds a real part to the panel impedances so that they will never identically equal zero. The transmission at coincidence is reduced by panel damping.

Coincidence has traditionally been used to describe the matching of the trace acoustic wave speed with the bending wave speed in single-layer panel. The usage of the term is extended in the present paper to refer to a matching between the acoustic field and *either* symmetric or antisymmetric panel motions that occur in a three-layer panel configuration. A reduction in panel TL can occur due to coincidence effects associated with either of the motion types. The design of a panel with increased TL must deal with coincidence associated with both types of panel deformation.

As indicated, the analytical description is idealized for panels of effectively infinite extent and plane-wave acoustic incidence and transmission. Transmission loss characteristics of finite panels mounted as partitions in walls will display effects due to panel resonances, which typically are more prominent at lower frequencies where there is a lesser modal overlap in the response of the panel resonances.

Coincidence for an individual finite panel resonance would occur when both frequency and surface wavelength of the incident acoustic field match the resonance frequency and corresponding wavelength of panel vibration. The mechanical impedance of the panel resonance nears zero when both the temporal and spacial characteristics of the excitation match those of the panel vibration.

Sound fields in reverberant rooms are generally diffuse in character, with sound propagating nearly uniformly at all angles of incidence with respect to a wall panel. The transmission coefficient is averaged over incidence orientation as follows:

$$\bar{\tau} = \int_0^{2\pi} \int_0^{\theta_{\text{lim}}} \tau(\theta,\phi) \sin\theta \cos\theta \, d\theta \, d\phi \times \left(\int_0^{2\pi} \int_0^{\theta_{\text{lim}}} \sin\theta \cos\theta \, d\theta \, d\phi \right)^{-1}.$$

The transmission loss is defined by

$$\text{TL} = -10 \log_{10}(\bar{\tau}) \text{ dB}. \tag{6}$$

For typical reverberant rooms, a value of θ_{lim} equal to 78° is used in performing numerical integrations according to Eqs. (6).[13]

A. Model of panel dynamics: Isotropic core

The panel dynamics are described in terms of bending and in-plane extensional deformation in the face sheets and shear and dilatational wave propagation in the homoge-

neous isotropic core material. Both transverse and in-plane displacements are matched at the interfaces between the core and face sheets. The shear and normal stresses in the core material at the interfaces act as excitations in the governing equations for panel bending and extensional deformation.

For incident acoustic plane-wave excitation, the governing equations for face sheet deformation depend only on position in the direction of propagation across the panel surface. For convenience, the in-plane x axis is oriented in the direction of propagation. For panel bending,

$$D\frac{\partial^4 w}{\partial x^4}+m\frac{\partial^2 w}{\partial t^2}=\Sigma \text{ normal stresses}$$

and for in-plane deformation (7)

$$E_{11}^{\text{fs}}t\frac{\partial^2 u}{\partial x^2}-m\frac{\partial^2 u}{\partial t^2}=\Sigma \text{ shear stresses.}$$

The normal stresses include those due to the core material and the external acoustic pressure at the panel surface. The shear stresses occur only at the face sheet/core interface. A moment about the neutral axis of the thin face sheets due to the core shear stresses that act at the surface is neglected. The signs of the stress and pressure terms on the right-hand side of Eqs. (7) depend on the sign convention and whether they act on the top or bottom surface of the face sheet.

For plane-wave incidence the plate displacements are functions of frequency and the acoustic trace wave number as follows:

$$w(x,t)=we^{i(kX-\omega t)},\quad u(x,t)=ue^{i(kX-\omega t)}. \tag{8}$$

Deformation in the core material is described in terms of shear and dilatational wave propagation in a homogeneous isotropic elastic medium. For the geometry of the panel TL problem, only a single term is required for the shear wave potential function. The dilatational wave equation is

$$(\lambda+2\mu)\frac{\partial^2\Phi}{\partial x^2}=\rho\frac{\partial^2\Phi}{\partial t^2}$$

and, for the shear wave equation, (9)

$$\mu\frac{\partial^2\psi}{\partial x^2}=\rho\frac{\partial^2\psi}{\partial t^2}.$$

The stress and displacement fields within the core are expressed in terms of the wave potentials by

$$\begin{aligned}
u&=\frac{\partial\Phi}{\partial x}-\frac{\partial\psi}{\partial z}, & \sigma_x&=\lambda\nabla^2\Phi+2\mu\left(\frac{\partial^2\Phi}{\partial x^2}-\frac{\partial^2\psi}{\partial x\,\partial z}\right),\\
v&=0, & \sigma_y&=\lambda\nabla^2\Phi,\\
w&=\frac{\partial\Phi}{\partial z}+\frac{\partial\psi}{\partial x}, & \sigma_z&=\lambda\nabla^2\Phi+2\mu\left(\frac{\partial^2\Phi}{\partial z^2}+\frac{\partial^2\psi}{\partial x\,\partial z}\right),\\
& & \tau_{xz}&=2\mu\frac{\partial^2\Phi}{\partial x\,\partial z}+\mu\left(\frac{\partial^2\psi}{\partial x^2}-\frac{\partial^2\psi}{\partial z^2}\right).
\end{aligned} \tag{10}$$

Consistent with acoustic plane-wave excitation, the shear and dilatational wave potentials have the following forms:

$$\begin{aligned}
\Phi_{\pm}&=A_{\pm}e^{i(kX\pm k_{zd}Z-\omega t)},\\
\psi_{\pm}&=B_{\pm}e^{i(kx\pm k_{zs}Z-\omega t)},
\end{aligned} \tag{11}$$

where the + and − signs are for waves propagating upward and downward through the core material, respectively. The in-plane wave number matches the trace acoustic wave number and the transverse wave numbers are found from the dispersion relationships for shear and dilatational waves as follows:

$$\begin{aligned}
&k^2+k_{zd}^2=k_d^2,\quad c_d=\omega/k_d=\sqrt{(\lambda+2\mu)/\rho},\\
&k^2+k_{zs}^2=k_s^2,\quad c_s=\omega/k_s=\sqrt{\mu/\rho}.
\end{aligned} \tag{12}$$

The core layer is described by a 4×4 impedance matrix that relates normal and shear stress amplitudes to transverse and in-plane velocity amplitudes at the top and bottom surfaces. The impedances are obtained by superimposing upward and downward propagating shear and dilatational waves, as given by Eq. (11). The unknown amplitudes of the wave potentials are eliminated through use of the displacement and stress relations in Eq. (9) to obtain the impedance expressions

$$\begin{Bmatrix}\sigma_{z,t}\\ \sigma_{z,b}\\ \tau_{xz,t}\\ \tau_{xz,b}\end{Bmatrix}=\begin{bmatrix}Z_{11}&Z_{12}&Z_{13}&Z_{14}\\ Z_{12}&Z_{11}&-Z_{14}&-Z_{13}\\ -Z_{13}&Z_{14}&Z_{33}&Z_{34}\\ -Z_{14}&Z_{13}&Z_{34}&Z_{33}\end{bmatrix}\begin{Bmatrix}\dot w_t\\ -\dot w_b\\ \dot u_t\\ -\dot u_b\end{Bmatrix}, \tag{13}$$

where

$$\begin{aligned}
Z_{11}&=(i\rho\omega/\Delta)[k^2k_{zs}\cos(k_{zs}L)\sin(k_{zd}L)\\
&\quad+k_{zs}^2k_{zd}\sin(k_{zs}L)\cos(k_{zd}L)],\\
Z_{12}&=(i\rho\omega/\Delta)[k_{zs}^2k_{zd}\sin(k_{zs}L)+k^2k_{zs}\sin(k_{zd}L)],\\
Z_{33}&=(i\rho\omega/\Delta)[k_{zd}^2k_{zs}\cos(k_{zs}L)\sin(k_{zd}L)\\
&\quad+k^2k_{zd}\sin(k_{zs}L)\cos(k_{zd}L)],\\
Z_{34}&=(i\rho\omega/\Delta)[k_{zd}k^2\sin(k_{zs}L)+k_{zd}^2k_{zs}\sin(k_{zd}L)],
\end{aligned} \tag{14}$$

$$\begin{aligned}
Z_{13}&=(k/\omega\Delta)\{k_{zs}k_{zd}(4\mu k^2-\rho\omega^2)\\
&\quad\times[1-\cos(k_{zd}L)\cos(k_{zs}L)]\\
&\quad+\sin(k_{zd}L)\sin(k_{zs}L)\\
&\quad\times[2\mu(k^4+k_{zd}^2k_{zs}^2)-\rho\omega^2k^2]\},\\
Z_{14}&=(\rho\omega kk_{zd}k_{zs}/\Delta)[\cos(k_{zd}L)-\cos(k_{zs}L)],
\end{aligned}$$

and

$$\begin{aligned}
\Delta&=2k^2k_{zd}k_{zs}[1-\cos(k_{zd}L)\cos(k_{zs}L)]\\
&\quad+(k^4+k_{zd}^2k_{zs}^2)\sin(k_{zd}L)\sin(k_{zs}L).
\end{aligned}$$

The impedance expressions for the core stresses, Eqs. (13), are combined with the equations for both face sheets, Eqs. (7), to give a system of four equations in terms of four unknown velocity amplitudes describing in-plane and transverse motions of the face sheets. The excitations are the acoustic pressures on the exterior sides of the face sheets. The equation for transverse displacements of the top face sheet becomes

$$\left(D\frac{k^4}{-i\omega}-i\rho\omega+Z_{11}+\frac{ikt}{2}Z_{13}\right)\dot{w}_1$$
$$-\left(Z_{12}-\frac{ikt}{2}Z_{14}\right)\dot{w}_2+Z_{13}\dot{u}_1-Z_{14}\dot{u}_2=-P_1.$$

For in-plane displacements of the top face sheet,

$$\left(E_{11}^{fs}t\frac{k^2}{-i\omega}-i\rho\omega+Z_{33}\right)\dot{u}_1-Z_{34}\dot{u}_2$$
$$+\left(\frac{ikt}{2}Z_{33}-Z_{13}\right)\dot{w}_1+\left(\frac{ikt}{2}Z_{34}-Z_{14}\right)\dot{w}_2=0.$$

For transverse displacements of the bottom face sheet,

$$-\left(Z_{12}-\frac{ikt}{2}Z_{14}\right)\dot{w}_1$$
$$+\left(D\frac{k^4}{-i\omega}-i\rho\omega+Z_{11}+\frac{ikt}{2}Z_{13}\right)\dot{w}_2$$
$$+Z_{14}\dot{u}_1-Z_{13}\dot{u}_2=P_2 \qquad (15)$$

and, for in-plane displacements of the bottom face sheet,

$$-Z_{34}\dot{u}_1+\left(E_{11}^{fs}t\frac{k^2}{-i\omega}-i\rho\omega+Z_{33}\right)\dot{u}_2$$
$$-\left(\frac{ikt}{2}Z_{34}-Z_{14}\right)\dot{w}_1-\left(\frac{ikt}{2}Z_{33}-Z_{13}\right)\dot{w}_2=0.$$

The terms containing $(ikt/2)\,\dot{w}$ account for an in-plane displacement at the core/face sheet interface that results from the rotation of the face sheet cross section during bending.

For panel configurations with identical face sheets, appropriately adding and subtracting Eq. (15) result in uncoupled equations for symmetric and antisymmetric behavior of the panel. The panel impedances Z_s and Z_a are given by

$$\frac{\dot{u}_s}{\dot{w}_s}=\left(Z_{13}-Z_{14}-\frac{ikt}{2}(Z_{33}-Z_{34})\right)$$
$$\times\left(E_{11}^{fs}t\frac{k^2}{-i\omega}-i\rho\omega+Z_{33}-Z_{34}\right)^{-1}=R_s,$$
$$Z_s=D(k^4/-i\omega)-i\rho\omega+Z_{11}+Z_{12}$$
$$+(ikt/2)(Z_{13}-Z_{14})+R_s(Z_{13}-Z_{14}), \qquad (16)$$

and

$$\frac{\dot{u}_a}{\dot{w}_a}=\left(Z_{13}+Z_{14}-\frac{ikt}{2}(Z_{33}+Z_{34})\right)$$
$$\times\left(E_{11}^{fs}t\frac{k^2}{-i\omega}-i\rho\omega+Z_{33}+Z_{34}\right)^{-1}=R_a,$$
$$Z_a=D(k^4/-i\omega)-i\rho\omega+Z_{11}-Z_{12}$$
$$+(ikt/2)(Z_{13}+Z_{14})+R_a(Z_{13}+Z_{14}).$$

The effects of damping are accounted for by allowing the stiffness moduli for the face sheets and core material to become complex. For instance, face sheet damping is characterized by a complex bending rigidity D^*, where $D^*=D(1-i\eta)$. Here, η is the damping loss factor for extensional deformation in the face sheet material. Different damping values can be used for shear and dilatational deformation in the core material.

In the absence of panel damping, zeros occur in the panel impedances where the trace acoustic wave speed matches the wave speed for freely propagating waves in the panel. This condition is referred to as acoustic coincidence and is of particular importance in describing the TL behavior of a panel.

The trace acoustic wave speed, which is defined by the trace wave number on the panel surface and frequency, is dependent on the angle of incidence of the acoustic plane wave as follows:

$$c_t=c_0/\sin\theta,\quad k=k_0\sin\theta,\quad c_t=\omega/k. \qquad (17)$$

Figure 2 shows calculated wave speeds for both symmetric and antisymmetric motions of a sandwich panel with $\frac{1}{4}$-in. plywood face sheets and a 3-in.-thick closed cell styrofoam core. The wave speeds were evaluated from zeros in the panel impedances without damping in either the face sheets or core. Small values of panel damping would shift slightly the location of a minima in the magnitude of impedance.

At low frequencies, symmetric motions of the panel are controlled by the stiffness of the core, they do not propagate freely with zero impedance. At higher frequency, near 1.5 kHz, the nearly vertical line indicates a freely propagating symmetric wave in the panel with large and very rapidly varying wave speed. This behavior is associated with a double wall resonance of the panel that is characterized by the mass of the face sheets in resonance against the stiffness of the core. The styrofoam core is lightweight with negligible mass in comparison with the face sheets.

The double wall resonance frequency is approximated by

$$f_{dw}\cong\frac{1}{2\pi}\left[\left(\frac{2(\lambda+2\mu)}{L}\right)\left(m+\frac{\rho L}{6}\right)^{-1}\right]^{1/2}. \qquad (18)$$

Face sheet motions are uniform at the double wall resonance, corresponding to zero trace wave number and infinite wave speed. An incident acoustic wave at normal incidence would coincidently excite symmetric panel motion for frequencies near the double wall resonance. Panel damping induced by thickness deformation in the core would limit the acoustic transmission.

At higher frequencies, panel wave speeds for both symmetric and antisymmetric motions approach a bending wave speed limit based on the bending rigidity of a face sheet as follows:

$$c=(D/m)^{1/4}\sqrt{\omega}. \qquad (19)$$

In addition to the face sheet bending region at higher frequencies, antisymmetric motions include a mid-frequency, core shear stiffness controlled region and a low-frequency bending region dependent on the bending rigidity for the entire panel cross section. In the midfrequency region, an approximate form for the panel wave speed is given by

$$c\cong\left[\left(\frac{2G}{L}\right)\left(m+\frac{\rho L}{2}\right)^{-1}\right]^{1/2} \qquad (20)$$

and is constant with frequency. For the low-frequency region, the limiting form in Eq. (19) applies but with D for an individual face sheet replaced by the appropriate expression for the panel as a whole as follows:

$$D'=E_{11}^{fs}t(L+t)^2/4. \qquad (21)$$

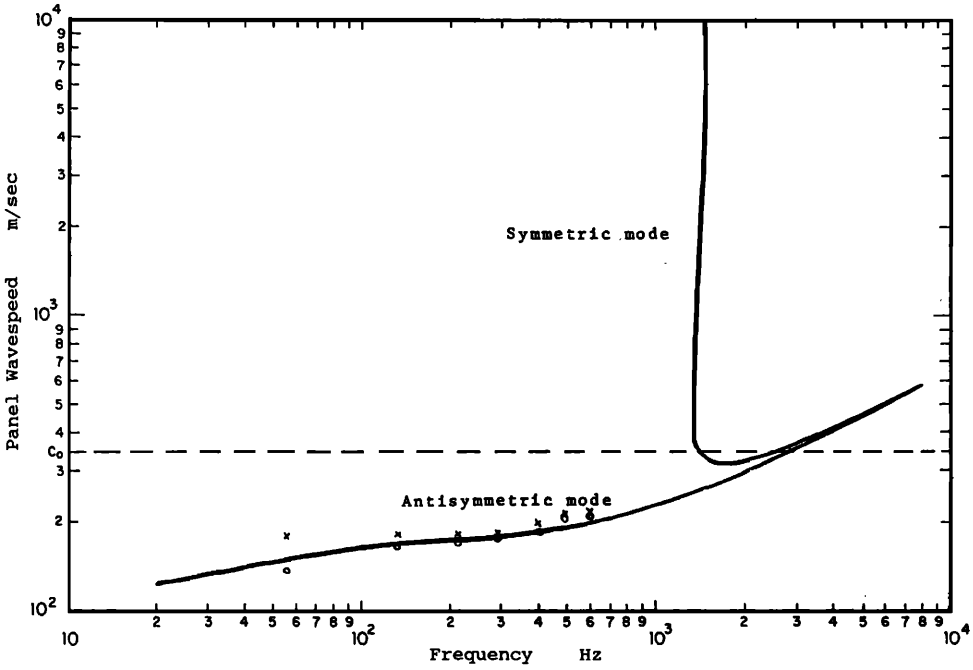

FIG. 2. Wave speeds for symmetric and antisymmetric motions in a sandwich panel with ¼-in. plywood face sheets and a 3-in. styrofoam core: ×—measured values from beam experiment assuming bending deformation; O—measured values assuming core shear deformation dominates.

The trace acoustic wave speed is represented in Fig. 2 parametrically as a function of the angle of incidence by a vertical line extending upward from the acoustic sound speed c_0. According to Eq. (17), the trace wave speed is always greater than c_0; it equals c_0 at grazing incidence, $\theta = 90°$, and becomes infinite at normal incidence $\theta = 0°$.

Coincidence occurs, therefore, when either the symmetric or antisymmetric panel wave speeds exceeds c_0 at an angle of incidence determined by the intersection of a vertical line and the wave speed plot for the panel motion. Frequencies where coincidence occurs will exhibit reduced TL as a result of the coincidence matching between the acoustic excitation and the panel response characteristics.

For the plywood/styrofoam panel of Fig. 2, reduced TL occurs near 1.3 kHz due to coincidence matching with symmetric panel motion near the double wall resonance and at higher frequencies, beginning near 3 kHz, for both symmetric and antisymmetric motions characterized by face sheet bending.

B. TL results: Isotropic core

Here, 4- by 8-ft test panels were fabricated for TL measurements in the TL facility at Massachusetts Institute of Technology. The facility consists of two adjacent 100-m^3 reverberation rooms where the common wall between the rooms consisted of a double walled 10-in.-thick brick construction that is isolated from the floor and ceiling by cork. The common floor and ceiling between the rooms was of 8-in.-thick concrete. Flanking path transmission was estimated by replacing the test panel with a "high" TL configuration consisting of 5¾-in.-thick gypsum panels with 1-in. fiberglass filled spaces as separations. The measured flanking path transmission, which indicates an upper bound on flanking transmission, i.e., a lower bound on flanking TL, is shown in Fig. 3.

Measured and predicted TL results for the ¼-in. plywood/3-in. styrofoam core configuration are shown in Fig. 3. Parameter values used in the predictions for the styrofoam material were determined experimentally, based on resonance frequency measurements with a thin layer of styrofoam sandwiched between rigid metal discs. Measure-

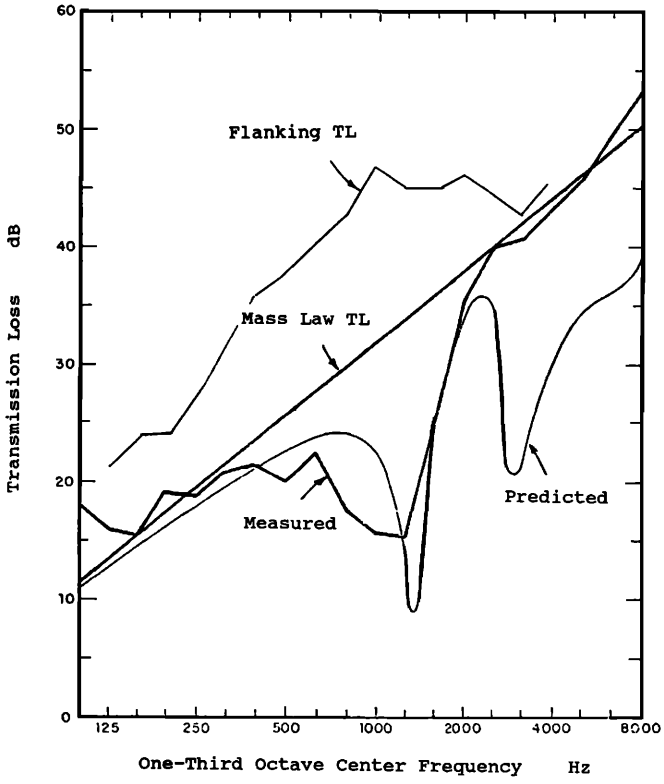

FIG. 3. TL results for the ¼-in. plywood/3-in. styrofoam panel: O—measured lower bound on flanking TL.

ments were made for modes of vibration involving both compressional and shear deformation of the styrofoam. Parameter values for the styrofoam are given in Table I.

Measurements were also performed on an 8-ft-long, 4-in.-wide beam section of the panel in order to provide additional confirmation of the material property values for the styrofoam. Resonance frequencies and mode shapes were measured with the beam freely supported. Wave-speed estimates, based on the frequency and wavelength for the beam modes, were compared with the predicted phase speeds, based on the values in Table I, with good agreement, as shown in Fig. 2.

Also shown in Fig. 3 is the predicted field incidence mass law TL line for a panel with the same total surface mass as the test panel. Limp wall mass law TL is used to scale the TL of a panel, and represents the performance of a panel with no rigidity or wavebearing capacity, i.e., a limp wall.

At low frequencies, below where coincidence occurs for the test panel, the measured and predicted TL results follow the mass law TL line. At very low frequencies, finite panel size effects result in deviations from mass law behavior. The measured coincidence dip in TL due to the double wall resonance for symmetric panel motions near 1.3 kHz is broader than predicted. This may also be attributable to finite panel size effects.

Anomalous behavior occurs at higher frequencies where the predicted coincidence dip near 3 kHz is not seen in the measured results. Coincidence near 3 kHz is associated with bending wave propagation in the individual face sheets with only an apparently small effect due to the shear and inertial properties of the core.

Concerns with orthotropic behavior in the plywood face sheets have been suggested by Ordubadi and Lyon[14] as a possible explanation for the discrepancy. Plywood is a composite laminate that exhibits different bending rigidities as a function of orientation or direction of propagation within the panel. This would tend to smear out in frequency effects in TL due to face sheet coincidence.

In addition, if the top and bottom face sheets are not similarly aligned, then an incident acoustic wave that is strongly transmitted through one face sheet at coincidence for a particular direction of propagation across the panel surface, would not coincidently transmit through the other face sheet. Higher panel damping levels above the estimated level of $n = 0.03$ would also increase the TL above coincidence, though it is not understood how damping levels could be 10 dB larger in order to increase the calculated TL to match the measured results.

A second test panel was fabricated with a $1\frac{1}{2}$-in.-thick styrofoam core. Predicted wave speeds for the panel are shown in Fig. 4 and measured and predicted TL results in Fig. 5. Reducing the thickness of the core, without changing its material properties, has two primary effects, as seen in the wave-speed plot; first, the stiffness of the core is increased, thereby shifting the double wall resonance to higher frequency, and second, the shear stiffness of the core is reduced,

TABLE I. Panel and core parameter values.

	Face sheet (plywood)	
$E^{fs}_{11} = 7\times10^9$ N/m^2		
m—varies with thickness and amount of glue used to bond to core		
Panel configuration	m	
1 $1\frac{1}{2}$-in. foam core $\frac{1}{4}$-in. plywood	4.0 kg/m^2	
2 3-in. foam core $\frac{1}{4}$-in. plywood	3.73 kg/m^2	
3 3-in. honeycomb No. 1 $\frac{1}{4}$-in. plywood	4.17 kg/m^2	
4 3 $\frac{5}{16}$-in. honeycomb No. 2 $\frac{3}{8}$-in. plywood	5.7 kg/m^2	
	Core material	
	Closed cell styrofoam	
	$\rho = 16$ kg/m^3 $\lambda + 2\mu = 1.25\times10^7$ N/m^2 $\mu = 3.1\times10^6$ N/m^2	
Honeycomb	No. 1	No. 2
Designation	18-$\frac{3}{4}$	11-1
ρ	28 kg/m^3	21 kg/m^3
E_{11}	4×10^6 N/m^2	4×10^5 N/m^2
E_{22}	$\cong E_{11}$	9.5×10^7 N/m^2
E_{33}	3.7×10^8 N/m^2	$\cong E_{11}$
$E_{12} = E_{13} = E_{23}$	4×10^5 N/m^2	4×10^4 N/m^2
E_{44}	5×10^7 N/m^2	7.6×10^6 N/m^2
E_{55}	2.3×10^7 N/m^2	1.7×10^5 N/m^2
E_{66}	2×10^5 N/m^2	4.2×10^6 N/m^2
η	0.03, 0.05	0.03

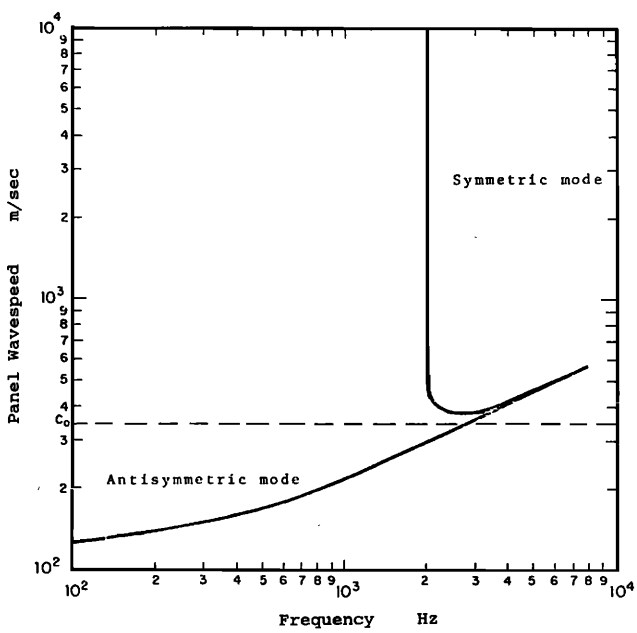

FIG. 4. Wave speeds for a $\frac{1}{4}$-in. plywood/1 $\frac{1}{2}$-in. styrofoam panel.

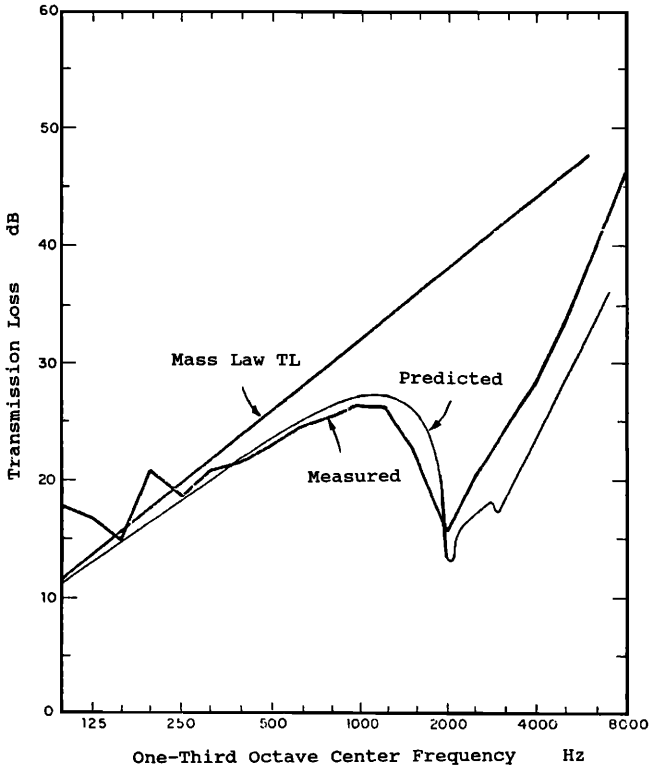

FIG. 5. TL results for the ¼-in. plywood/1 ½-in. styrofoam panel.

lowering the wave speed in the midfrequency region for antisymmetric panel motions. The shift in double wall resonance frequency has a direct effect on the TL in that the associated coincidence dip is moved to higher frequency.

A reduction in the shear stiffness for the thinner core does not have a noticeable effect on the TL. Coincidence effects associated with antisymmetric panel motions are dependent on bending deformation in an individual face sheet and occur in the high-frequency region. If the core was appreciably increased in thickness, resulting in an increase in shear stiffness so that the midfrequency wave speed exceeded the sound speed, then coincidence would be shifted to lower frequencies with a pronounced effect on TL.

The discrepancy at and above face sheet coincidence occurs for the 1½-in. panel, though not to the same degree. Coincidence for symmetric and antisymmetric motions occur closer to each other for the thinner panel configuration.

C. Model of panel dynamics: Orthotropic core

Honeycomb materials are commonly used in the fabrication of sandwich panel constructions. Such materials have different stiffness moduli in planes perpendicular and parallel to the direction of the cells, and can be characterized as orthotropic with nine independent stiffness constants. The development in this section assumes that one of the principal axes for the orthotropic core is aligned perpendicular to the plane of the panel.

Impedance expressions are developed for symmetric and antisymmetric panel motions as in Sec. I B. The approach differs from that in Sec. I B in that an initial displacement field is assumed for the core and both face sheets. Elastic potential and kinetic energies are evaluated in terms of the displacements and Lagrange's equation is utilized to obtain the system equations for the unknown displacement amplitudes. Virtual work contributions due to symmetric and antisymmetric pressure distributions on the outer surfaces of the face sheets are excitations that allow solution of the system equations in terms of the panel impedances Z_s and Z_a.

The initial displacement field is harmonic in time and in the direction of propagation of the incident acoustic wave over the surface of the panel. The displacements vary linearly through the thickness of the panel. The assumed displacement field is identical to that introduced by Ford *et al.*[6] For the symmetric displacement field:

$$u_1 = \beta_s \cos(kx) - \left(z - \frac{L}{2}\right)\frac{\partial w_1}{\partial x}, \tag{22}$$

$$v_1 = 0,$$

$$w_1 = \alpha_s \sin(kx),$$

for the upper face sheet;

$$u_2 = [\beta_s + \zeta \cos(\pi z/L)]\cos(kx),$$

$$v_2 = 0,$$

$$w_2 = (2\alpha_s/L) z \sin(kx),$$

for the core; and

$$u_3 = \beta_s \cos(kx) - \left(z + \frac{L}{2}\right)\frac{\partial w_3}{\partial x},$$

$$v_3 = 0,$$

$$w_3 = -\alpha_s \sin(kx),$$

for the lower face sheet.

For the antisymmetric displacement field:

$$u_1 = \beta_a \cos(kx) - \left(z - \frac{L}{2}\right)\frac{\partial w_1}{\partial x},$$

$$v_1 = 0,$$

$$w_1 = \alpha_a \sin(kx),$$

for the upper face sheet;

$$u_2 = (2\beta_a/L) z \cos(kx),$$

$$v_2 = 0,$$

$$w_2 = \alpha_a \sin(kx),$$

for the core; and

$$u_3 = -\beta_a \cos(kx) - \left(z + \frac{L}{2}\right)\frac{\partial w_3}{\partial x},$$

$$v_3 = 0,$$

$$w_3 = \alpha_a \sin(kx), \tag{23}$$

for the lower face sheet.

The amplitudes β and α describe in-plane and transverse displacements in the panel, respectively. The in-plane displacements terms for the face sheets that are proportional to $\partial w/\partial x$ account for the rotation of the cross section of the face sheet during bending deformation. The displacement amplitude ζ in the symmetric displacement field allows for waves that propagate in-plane within the core.

Elastic strains are determined from the displacements according to the following:

$$\epsilon_x = \frac{\partial u}{\partial x}, \quad \epsilon_y = \frac{\partial v}{\partial y}, \quad \epsilon_z = \frac{\partial w}{\partial z},$$
$$\gamma_{xy} = \frac{\partial u}{\partial y} + \frac{\partial v}{\partial x}, \quad \gamma_{xz} = \frac{\partial u}{\partial z} + \frac{\partial w}{\partial x}, \tag{24}$$
$$\gamma_{yz} = \frac{\partial v}{\partial z} + \frac{\partial w}{\partial y}.$$

The elastic potential energy density W is given by

$$2W = E_{11}\epsilon_x^2 + 2E_{12}\epsilon_x\epsilon_y + 2E_{13}\epsilon_x\epsilon_z + E_{22}\epsilon_y^2 + 2E_{23}\epsilon_y\epsilon_z + E_{33}\epsilon_z^2 + E_{44}\gamma_{xy}^2 + E_{55}\gamma_{xz}^2 + E_{66}\gamma_{xy}^2. \tag{25}$$

For the orthotropic core, stresses are related to the strains by the symmetric stiffness matrix as follows:

$$\begin{Bmatrix} \sigma_x \\ \sigma_y \\ \sigma_x \\ \gamma_{yz} \\ \gamma_{xz} \\ \gamma_{xy} \end{Bmatrix} = \begin{Bmatrix} E_{11} & E_{12} & E_{13} & 0 & 0 \\ & E_{22} & E_{23} & 0 & 0 \\ & & E_{33} & 0 & 0 \\ & & & E_{44} & 0 \\ & & & & E_{55} \end{Bmatrix} \begin{Bmatrix} 0 & \epsilon_x \\ 0 & \epsilon_y \\ 0 & \epsilon_z \\ 0 & \gamma_{yz} \\ 0 & \gamma_{xz} \\ E_{66} & \gamma_{xy} \end{Bmatrix}. \tag{26}$$

For the isotropic face sheets, the stiffnesses in Eqs. (26) are described in terms of the Lamé constants for the material by

$$E_{11} = E_{22} = E_{33} = \lambda + 2\mu,$$
$$E_{12} = E_{13} = E_{23} = \lambda, \tag{27}$$
$$E_{44} = E_{55} = E_{66} = \mu.$$

Potential energies for use in Lagrange's equations are evaluated for both face sheets and the core by integrating the potential energy density over a volume defined by the thickness of the panel component in the z direction, one wavelength of the incident acoustic wave in the x direction, and per unit distance in the y direction. The total potential energies are in terms of the parameters α_s, β_s, and ζ for symmetric panel motions and α_a and β_a for antisymmetric motions.

The displacement fields in the face sheets have been formulated so that the shear strain γ_{xz} and shear stress σ_{xz} equal zero. The effects of transverse shear deformation in the face sheets are not included in the model. The potential energy expression only accounts for in-plane stretching associated with either bending or in-plane extensional deformation.

Kinetic energies are similarly defined in terms of volume integrals as follows:

$$\mathrm{KE} = \frac{1}{2}\int \rho(\dot{u}^2 + \dot{v}^2 + \dot{w}^2)\, d\,\mathrm{Vol}. \tag{28}$$

The effects of rotary inertia are included in the kinetic energy expressions for the face sheets.

Lagrange's equation is utilized to generate the system equations describing the dynamics of the sandwich panel as follows:

$$\left(\frac{d}{dt}\right)\left(\frac{\partial \mathrm{KE}}{\partial \dot{q}_r}\right) - \frac{\partial \mathrm{KE}}{\partial q_r} + \frac{\partial \mathrm{PE}}{\partial q_r} = Q_r, \tag{29}$$

where KE and PE are the total kinetic and potential energies for both face sheets and the core. Here, q_r are the generalized displacements and include α_s, β_s, and ζ for symmetric panel motions, and α_a and β_a for antisymmetric panel motions. Also, $\dot{q}_r$ are the time derivatives of the generalized displacements.

In Eq. (29), Q_r are the generalized forces due to the acoustic pressures acting on the outer faces of the panel. For symmetric motion, a pressure $P_s \sin(kx)$ acts on the top and bottom surfaces of the panel. The corresponding virtual displacement is $\delta\alpha_s \sin(kx)$. The virtual work is evaluated over an area on both the top and bottom panel surfaces defined by one wavelength, λ in the x direction and per unit distance in the y direction, consistent with the surface dimensions used in the volume integral to obtain the kinetic and potential energies. Evaluating the generalized force terms from the virtual work yields the expression $P_s\lambda$ for symmetric motion and an identical expression for antisymmetric motion with P_a replacing P_s.

Lagrange's equations for symmetric motions with harmonic $e^{-i\omega t}$ time dependence yield the following symmetric matrix equations:

$$\{M_s\}\begin{Bmatrix} \alpha_s \\ \beta_s \\ \zeta \end{Bmatrix} = \begin{Bmatrix} -P_s \\ 0 \\ 0 \end{Bmatrix},$$

where

$$\{M_s\} = \begin{Bmatrix} \left[\frac{2E_{33}}{L} + \frac{E_{55}k^2L}{6} + \frac{E_{11}^{fs}k^4t^3}{3}\right] & \left[-E_{13}k - \frac{E_{11}^{fs}k^3t^2}{2}\right] & \left[-\frac{2E_{13}k}{\pi} - \frac{2E_{55}k}{\pi}\right] \\ \left[-\frac{\rho\omega^2L}{6} - m\omega^2\left(1 + \frac{k^2t^2}{3}\right)\right] & \left[+\frac{m\omega^2kt}{2}\right] & \\ & \left[E_{11}^{fs}k^2t + \frac{E_{11}k^2L}{2}\right] & \left[\frac{E_{11}k^2L}{\pi} - \frac{\rho\omega^2L}{\pi}\right] \\ & \left[-\frac{\rho\omega^2L}{2} - m\omega^2\right] & \\ & & \left[\frac{E_{11}k^2L}{4} + \frac{E_{55}\pi^2}{4L} - \frac{\rho\omega^2L}{4}\right] \end{Bmatrix}. \tag{30}$$

For antisymmetric panel motions, the system equations become:

$$\{M_a\}\begin{Bmatrix}\alpha_a\\ \beta_a\end{Bmatrix}=\begin{Bmatrix}-P_a\\ 0\end{Bmatrix},$$

where

$$\{M_a\}=\begin{bmatrix}\left[\dfrac{E_{55}k^2L}{2}+\dfrac{E_{11}^{fs}k^4t^3}{3}-\dfrac{\rho\omega^2L}{2}-m\omega^2\left(1+\dfrac{k^2t^2}{3}\right)\right] & \left[E_{55}k-\dfrac{E_{11}^{fs}k^3t^2}{2}+\dfrac{m\omega^2kt}{2}\right]\\ \left[E_{11}^{fs}k^2t+\dfrac{E_{11}k^2L}{6}+\dfrac{2E_{55}}{L}-\dfrac{\rho\omega^2L}{6}-m\omega^2\right] & \end{bmatrix}. \tag{31}$$

The dependence of panel dynamics on the direction of propagation in the plane of the panel relative to the principal axes of the orthotropic core material is straightforwardly described by transforming the principal axis stiffnesses to an axis system rotated in the plane of the panel by the azimuthal angle ϕ. Here, $\phi = 0$ corresponds to the x principal axis direction, see Fig. 6.

The displacement fields in Eqs. (22) and (23) are applied in the rotated axis system in identical form. The expressions for the kinetic and potential energies are also identical in form, as are the final matrix equations. The core stiffnesses E_{11}, E_{13}, E_{33}, and E_{55} need only be replaced by transformed values.

The stiffnesses in the rotated axis system are obtained in terms of the direction cosines for the rotation through angle ϕ as follows:[15]

$$\begin{aligned}\overline{E}_{11}&=l^4E_{11}+2l^2m^2E_{12}+m^4E_{22},\\ \overline{E}_{13}&=l^2E_{13}+m^2E_{23},\\ \overline{E}_{33}&=E_{33},\\ \overline{E}_{55}&=m^2E_{44}+l^2E_{55},\end{aligned} \tag{32}$$

where the direction cosines are given by $l=\cos\phi$ and $m=\sin\phi$.

Finally, the panel dynamics are described in terms of symmetric and antisymmetric impedances that are obtained by inverting the system matrix equations as follows:

$$Z_s=-P_s/-i\omega\alpha_s,\quad Z_a=-P_a/-i\omega\alpha_a. \tag{33}$$

The transmission coefficient and TL are then evaluated from Eqs. (4) and (6).

D. TL results: Orthotropic core

A test panel was fabricated with $\frac{1}{4}$-in. plywood face sheets and a 3-in.-thick resin-impregnated paper honeycomb core. The cells of the honeycomb were aligned perpendicular to the plane of the panel. The orthotropic behavior of the honeycomb involves nine independent material stiffnesses. Estimates of material stiffnesses were obtained from resonance frequency measurements on a test sample consisting of a thin layer of honeycomb sandwiched between rigid metal disks. Such tests gave values for the main diagonal axial stiffness E_{11}, E_{22}, and E_{33}, as well as the shear stiffnesses

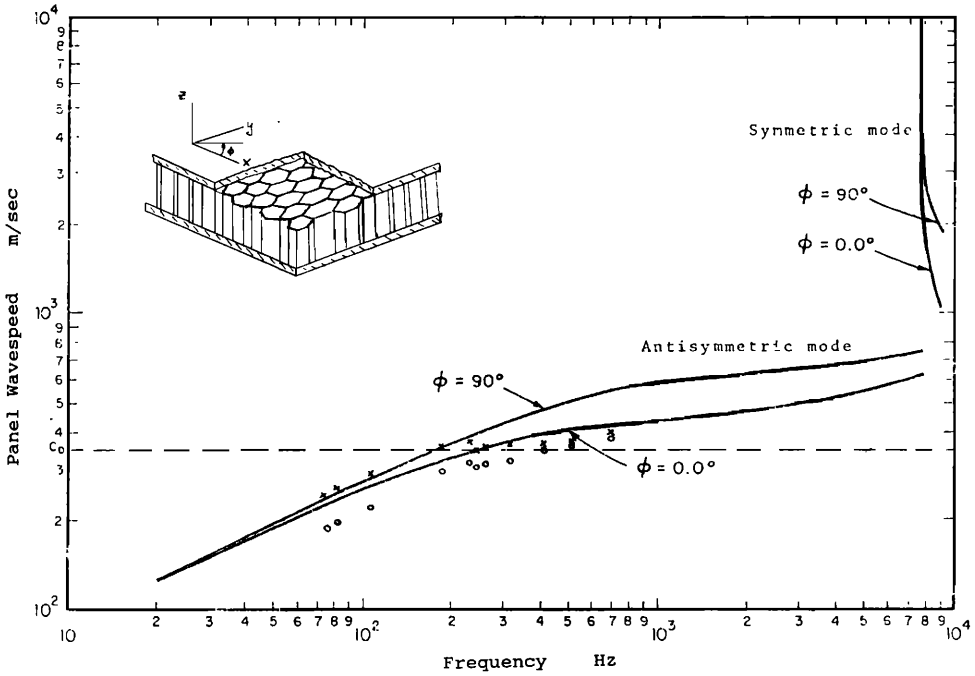

FIG. 6. Wave speeds for symmetric and antisymmetric motions in a sandwich panel with 3-in. honeycomb core (No. 1) and $\frac{1}{4}$-in. plywood face sheets: ×—measured values from beam experiment ($\phi = 0°$ orientation of honeycomb) assuming bending deformation; O—measured values assuming core shear deformation dominates.

E_{44}, E_{55}, and E_{66}. The off-diagonal stiffnesses E_{13}, E_{23}, and E_{12} were arbitrarily assumed to be equal to 0.1 times the softer of the axial stiffnesses. Transmission loss predictions were not found to be highly sensitive to the values of the off-diagonal stiffnesses. Parameter values for the honeycomb materials tested are given in Table I.

Wave-speed measurements on an 8-ft-long by 4-in.-wide beam section of the panel yielded results consistent with the parameter values in Table I. Predicted and measured wave speeds are shown in Fig. 6. The measurements were made with honeycomb material No. 1 in the $\phi = 0°$ orientation.

The wave speed for the orthotropic core is dependent on the direction of propagation of the incident acoustic wave relative to the principal axes within the honeycomb. For antisymmetric motions of the panel, the same low-, mid-, and high-frequency regions occur, as were observed for the styrofoam core panel. Owing to the large shear stiffnesses, E_{44} and E_{55}, of the honeycomb with the cells oriented perpendicular to the panel, the transition to the high-frequency region occurs above the audio frequency range. The differences in the mid-frequency region as a function of ϕ are due to the difference in the shear stiffnesses E_{44} and E_{55}.

Freely propagating symmetric panel motions do not occur until the region near the double wall resonance. The large value for the stiffness E_{33}, coupled with the light weight of the plywood face sheets, places the double wall resonance at high frequency, as seen in Fig. 6.

Coincidence effects for the honeycomb panel would be expected at low frequencies near 150–200 Hz associated with antisymmetric motion of the panel, and again at high frequencies, near 8 kHz, associated with the symmetric double wall resonance.

Predicted and measured TL results are shown in Fig. 7. The predictions were generated for two different values of damping loss factor for the core. The dip in TL due to coincidence is predicted for the region near 200 Hz, consistent with the wave-speed plot. Above the onset of coincidence, the TL rises at a rate that is influenced by damping. Increased damping levels increase the TL of the panel.

The measured TL results agree well with the predictions. At low frequencies, the discrepancies may be attributable to finite panel size effects. The honeycomb panel is inherently stiffer than the styrofoam panel so that finite panel effects would be expected to extend to somewhat higher frequency, as observed.

The minor reduction in TL near 6.3 kHz may, in somewhat uncertain terms, be the result of the double wall resonance, though the prediction hints at the effect at somewhat higher frequency.

E. Conclusions on panel TL behavior

Panel TL behavior is conveniently explained in terms of coincidence effects associated with motions in the panel that are either symmetric or antisymmetric in character. The decomposition into symmetric and antisymmetric motions is exact for symmetric panel constructions with identical face sheets and a homogeneous core material.

When the wave speed for either motion in the panel exceeds the sound speed, then a matching condition occurs

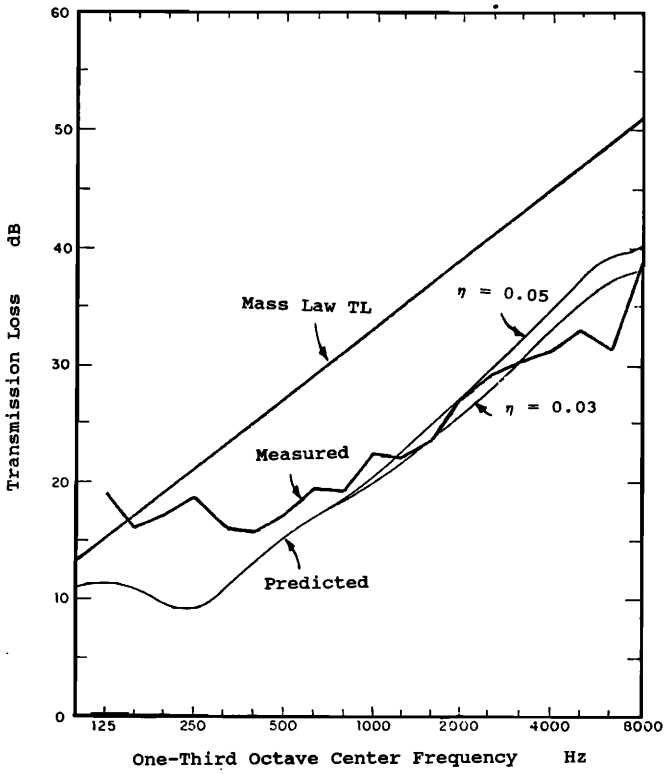

FIG. 7. TL results for the ¼-in. plywood/3-in. honeycomb (No. 1) sandwich panel.

between that motion in the panel and the incident acoustic wave that results in increased transmission through the panel. For symmetric panel motions, this occurs due to a double wall resonance, and at higher frequencies where the motion is controlled by bending deformation in the face sheets. For antisymmetric panel motions, three regions exist with bending deformation of the entire panel cross section: the controlling factor at low frequencies; the core shear stiffness controls in the mid-frequency transition region; and bending deformation in the face sheets is the limiting behavior at high frequencies. The wave speed for antisymmetric motions increases monotonically with frequency through the three regions. Where coincidence first occurs is importantly dependent on the shear stiffness in the core. If the stiffness is too large, coincidence can easily be shifted to occur below the mid-frequency region at lower frequencies with the TL adversely decreased over the useful frequency range.

This behavior has been demonstrated analytically and experimentally for panels with isotropic and orthotropic core materials. The next section discusses an approach for maintaining the TL performance of a panel in a design that also provides acceptable mechanical load bearing capacity.

II. IMPROVED TL PANEL DESIGN

The panel configurations discussed in the previous sections have serious deficiencies in TL in the principal speech bands from 500 Hz–2 kHz. The deficiencies were associated with different motions in the panel. For one design, the double wall resonance frequency and, coincidently, excited symmetric panel motions resulted in reduced TL, while for the

other, the honeycomb panel, coincidence of antisymmetric panel motions due to the large shear stiffness of the honeycomb core degraded performance.

Existing approaches to the design of high TL panels include the "shear wall" and the "coincidence wall." For the shear wall design, the double wall resonance is kept at high frequencies above the band of interest by employing a core with a large stiffness through the thickness of the panel. The shear stiffness is carefully controlled so that the wave speed in the mid-frequency region does not exceed the sound speed. Coincidence occurs at higher frequencies due to face sheet bending. Coincidence associated with both symmetric and antisymmetric panel motions is delayed to higher frequencies. In the principal speech bands, neither motion is coincidently excited and near mass law TL levels are achieved.

For the coincidence wall the double wall resonance is again kept at high frequencies. The approach differs from the shear wall in that panel damping is utilized to increase the TL in regions where antisymmetric panel motions are coincidently excited. In fact, there is benefit in having the core shear stiffness as large as possible, provided that significant damping levels can also be achieved within the core. Additional viscoelastic material layers are included within the core to provide damping. The difficulty is in achieving the required stiffness and damping levels. Transmission loss levels that are greater than mass law values are obtainable for an appropriately designed panel.

A. Mode canceling high TL panel design

An alternative design approach[9] is suggested here for which the double wall resonance frequency is moved to lower frequencies below the frequency band of interest. The core shear stiffness, as in the shear wall design, is limited so coincidence for antisymmetric panel motion is delayed and occurs above the band of interest. Coincidence at higher frequencies is the result of face sheet bending for both symmetric and antisymmetric panel motions.

In the band of interest, neither motion is coincidently excited and the TL is not degraded. The TL can exceed mass law values as a result of a cancellation of symmetric and antisymmetric motions of the face sheet on the opposite side from the incident sound field. The responses of both the symmetric and antisymmetric panel modes are mass controlled for all angles of incidence. On the incident face sheet, symmetric and antisymmetric motions are of similar phase relative to the acoustic excitation, depending on relative damping levels. On the transmitting face sheet, the motions to be superimposed are nearly out of phase and will cancel each other thereby reducing the actual motion and transmitted acoustic levels.

The acoustic behavior is comparable to conventional double wall designs where, above the double wall resonance, significant increases in TL at the rate of up to 18 dB/octave are predicted with more usual 12 dB/octave increases observed experimentally.

The double wall design with an air layer between the face sheets requires added structural elements, i.e., studs, for support. Transmission loss performance can suffer as a result of transmission through the studding, and if acoustic resonances in the air layer are not properly damped with fiberglass or other sound absorbing materials.

The proposed design maintains mechanical load bearing capacity primarily as a result of the shear stiffness of the core. While limited to avoid coincidence in the mid-frequency region, the shear stiffness is sufficiently large to provide mechanical support for the panel.

A physical embodiment of the proposed design is shown in Fig. 8. The honeycomb material has been oriented such that the cells lie in the plane of the panel. The stiffness in the thickness direction is substantially less than in the original orientation, which results in a lowering of the double wall resonance frequency. The shear stiffness is maintained for panel motions propagating in the y direction, as shown. The shear stiffness for propagation in the x direction, across the cells, is quite small.

A less stiff honeycomb configuration (No. 2) with larger cells and reduced resin content was required in fabricating a test panel to conform to the proposed design approach. The original material (No. 1) was too stiff; the double wall resonance with $\frac{1}{4}$-in. face sheets occurred near 800 Hz and the large shear stiffness for the in-plane y direction resulted in antisymmetric motions becoming coincident at low frequency near 250 Hz. The material finally chosen had 1-in. cells in comparison with the original $\frac{3}{4}$-in. size, and the resin content was reduced from 18% to 11%. To additionally lower the double wall resonance frequency, heavier $\frac{3}{8}$-in.-thick plywood face sheets were used in fabricating the 4- by 8-ft test panel. Heavier face sheets also lower the wave speed for antisymmetric motions in the mid-frequency region.

Transmission loss results are shown in Fig. 9. The measured TL values were large in comparison with the flanking TL values for the TL facility. The actual measured TL levels are shown, along with estimates of levels, if flanking transmission were removed. The band between the two results represents an uncertainty in the measured panel performance.

Greater than mass law TL was measured over nearly a decade in frequency from 250 Hz to 2.5 kHz. The discrepancy previously noted between measured and predicted results in the region of face sheet coincidence at higher frequencies occurs again in pronounced fashion.

A summary of the acoustic TL performance of the different panel configurations is shown in Table II. Single-num-

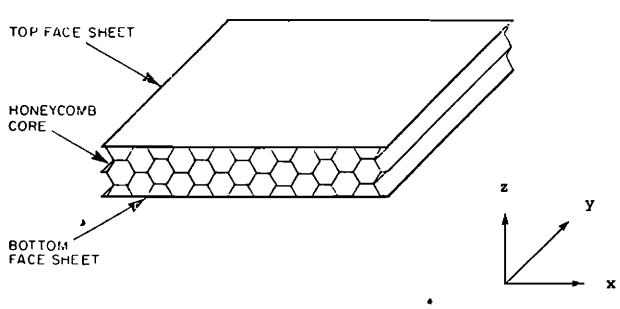

FIG. 8. Mode canceling panel with a honeycomb core.

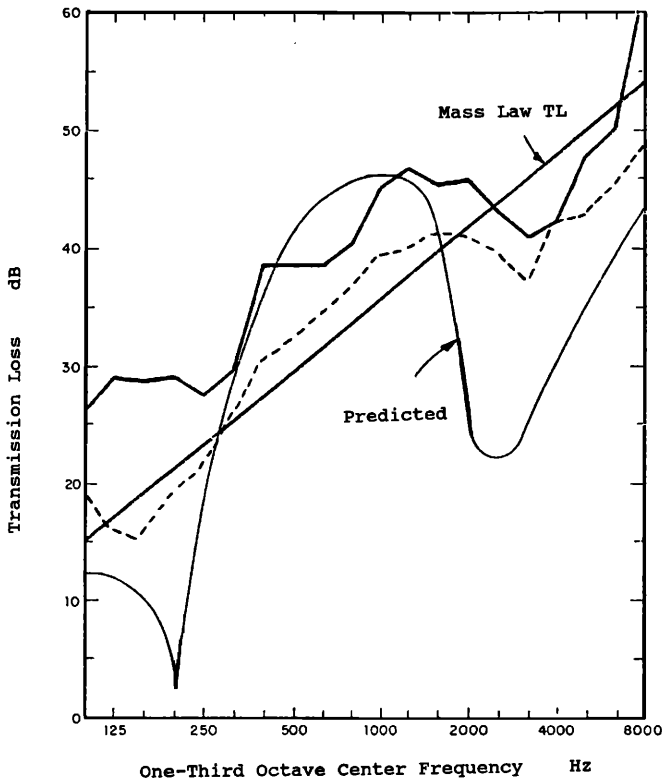

FIG. 9. TL results for the mode canceling panel: ----- measured TL results with correction for flanking transmission; – – – measured TL with no correction.

ber sound transmission class (STC) ratings for each panel were developed from the measured TL results. The proposed panel design resulted in an 11.5- to 17.5-dB improvement in STC rating. The greater weight of the new panel design contributes only 3.5 dB to the improvement.

B. Mechanical performance

A concern arises for the panel in that the design approach involves softening the core material. To assess the mechanical load bearing capacity of the panel, static deflections were calculated for a uniform load on one surface of a 4- by 8-ft panel section with assumed simple supports for both face sheets on all edges. The assumed boundary conditions for in-plane motion correspond to free edges. The displacement field for the face sheets and core match that of Eqs. (22) and (23) in both of the in-plane directions.

The expressions for symmetric panel displacements are:

$$u_1 = \beta_s \cos(k_x x)\sin(k_y y) - \left(z - \frac{L}{2}\right)\frac{\partial w_1}{\partial x}, \qquad (34)$$

$$v_1 = \gamma_s \sin(k_x x)\cos(k_y y) - \left(z - \frac{L}{2}\right)\frac{\partial w_1}{\partial y},$$

$$w_1 = \alpha_s \sin(k_x x)\sin(k_y y),$$

for the top face sheet;

$$u_2 = [\beta_s + \zeta_x \cos(\pi z/L)]\cos(k_x x)\sin(k_y y),$$

$$v_2 = [\gamma_s + \zeta_y \cos(\pi z/L)]\sin(k_x x)\cos(k_y y),$$

$$w_2 = (2\alpha_s/L) z \sin(k_x x)\sin(k_y y),$$

for the core;

$$u_3 = \beta_s \cos(k_x x)\sin(k_y y) - \left(z + \frac{L}{2}\right)\frac{\partial w_3}{\partial x},$$

$$v_3 = \gamma_s \sin(k_x x)\cos(k_y y) - \left(z + \frac{L}{2}\right)\frac{\partial w_3}{\partial y},$$

$$w_3 = -\alpha_s \sin(k_x x)\sin(k_y y),$$

for the bottom face sheet.

For antisymmetric panel displacements:

$$u_1 = \beta_a \cos(k_x x)\sin(k_y y) - \left(z - \frac{L}{2}\right)\frac{\partial w_1}{\partial x}, \qquad (35)$$

$$v_1 = \gamma_a \sin(k_x x)\cos(k_y y) - \left(z - \frac{L}{2}\right)\frac{\partial w_1}{\partial y},$$

$$w_1 = \alpha_a \sin(k_x x)\sin(k_y y),$$

for the top face sheet;

TABLE II. Summary of transmission loss results.

Panel configuration	Panel m	Mass law TL at 100 Hz	STC
1 1 $\frac{1}{2}$-in. foam core $\frac{1}{4}$-in. plywood	8.6 kg/m^2	11.5 dB	19
2 3-in. foam core $\frac{1}{4}$-in. plywood	8.7 kg/m^2	11.5 dB	20
3 3-in. honeycomb No. 1 $\frac{1}{4}$-in. plywood	10.5 kg/m^2	13.0 dB	22.5
Mode canceling panel design			
4 3 $\frac{5}{16}$-in. honeycomb No. 2 $\frac{3}{8}$-in. plywood (corrected for flanking)	13.0 kg/m^2	15.0 dB	41
5 3 $\frac{5}{16}$-in. honeycomb No. 2 $\frac{3}{8}$-in. plywood (uncorrected)	13.0 kg/m^2	15.0	35

$$u_2 = (2\beta_a/L)z\cos(k_x x)\sin(k_y y),$$
$$v_2 = (2\gamma_a/L)z\sin(k_x x)\cos(k_y y),$$
$$w_2 = \alpha_a \sin(k_x x)\sin(k_y y),$$

for the core;

$$u_3 = -\beta_a \cos(k_x x)\sin(k_y y) - \left(z + \frac{L}{2}\right)\frac{\partial w_3}{\partial x},$$
$$v_3 = -\gamma_a \sin(k_x x)\cos(k_y y) - \left(z + \frac{L}{2}\right)\frac{\partial w_3}{\partial y},$$
$$w_3 = (2\alpha_a/L)z\sin(k_x x)\sin(k_y y),$$

for the bottom face sheet. The wavenumbers k_x and k_y are restricted to integer multiples corresponding to the mode shapes of a finite simply supported panel as follows:

$$k_x = n\pi/h_x, \quad k_y = m\pi/h_y. \tag{36}$$

The uniform load on the top face sheet is expanded in terms of the mode shapes for transverse displacement of the face sheets as follows:

$$f(x,y) = \sum F_{mn} \sin\left(\frac{n\pi x}{h_x}\right)\sin\left(\frac{m\pi y}{h_y}\right). \tag{37}$$

Lagrange's equation is used to obtain the displacements in response to the uniform static load. Potential energies for symmetric and antisymmetric loadings are evaluated from the above displacement fields in the face sheets and core. The uniform loading on the top face, with amplitude f_1, is equivalent to symmetric and antisymmetric load amplitudes of $f_1/2$, according to Eqs. (1). The virtual work and generalized force is obtained by multiplying the load distributions by virtual transverse displacements for the top and bottom face sheets with the same distribution in x and y, and integrating over the full surface area of the panel. The potential energy is integrated over the full volume.

The orthogonality of the assumed displacement fields, along with Lagrange's equation, results in a set of uncoupled equations for the modal amplitudes of the displacements in terms of the amplitude of the uniform load. The matrix equations are solved for the transverse displacement amplitudes and the total displacements evaluated from the summations as follows:

$$W_s = \sum_n \sum_m \alpha_s^{n,m} \sin\left(\frac{n\pi x}{h_x}\right)\sin\left(\frac{m\pi y}{h_y}\right), \tag{38}$$
$$W_a = \sum_n \sum_m \alpha_a^{n,m} \sin\left(\frac{n\pi x}{h_x}\right)\sin\left(\frac{m\pi y}{h_y}\right).$$

The total displacement of the top and bottom face sheets is obtained by superimposing symmetric and antisymmetric terms as follows:

$$w_1 = (w_s + w_a)/2, \quad w_2 = (w_a - w_s)/2. \tag{39}$$

The expansions in Eqs. (38) are suitably truncated in evaluating the maximum displacement at the middle of the panel. With a 40 lb/sq ft load on the 4- by 8-ft panel, the calculated deflections are shown in Table III. Unfortunately, actual measurements of panel deflections were not carried out.

The orientation of the cells is of importance because the panel is rectangular, and not square. The stiffest configuration is with the larger of the shear stiffnesses aligned in the shorter panel direction. The dependence on orientation, in relation to the core shear stiffness, also implies that transverse shear deformation is of importance for the relatively long wavelength loading in this case.

TABLE III. Calculated panel deflections under uniform static load. Mode canceling panel design: 4- by 8-ft panel, 40-lb_f/ft^2 load on the top face.

Orientation of the core[a]	Deflection[b] at the center of the: top face sheet	bottom face sheet
$\phi = 0°$	0.2 in.	0.197 in.
$\phi = 45°$	0.05 in.	0.048 in.
$\phi = 90°$	0.037 in.	0.035 in.

[a] For $\phi = 0°$, the smaller shear stiffness is aligned with the smaller panel dimension, the cells point in the long dimension.
[b] Symmetric and antisymmetric deflection components are obtained by, respectively, subtracting and adding the top and bottom deflections, and dividing by 2, as indicated in Eq. (2).

The dependence on orientation could be avoided by fabricating the core from a quilt-like arrangement of blocks of honeycomb with the cells alternately pointing at right angles to each other. The effective core shear stiffness would be an average of the values for the honeycomb in the two in-plane directions.

The symmetric deflections are small by comparison with the antisymmetric terms. Symmetric deflection of the panel is very weakly dependent on the dimensions of the panel; it is primarily determined by the axial stiffness of the core material. Antisymmetric deflections are the result of bending deformation of the panel and depend very importantly on its dimensions.

ACKNOWLEDGMENTS

The authors wish to thank the National Science Foundation for their financial support of this work. Nathan Martin is also thanked for helpful recommendations made during the course of this study.

[1] B. G. Watters and G. Kurtze, "New Wall Design for High Transmission Loss or High Damping," J. Acoust. Soc. Am. **31**, 739–748 (1959).
[2] G. Warnaka, US Patent No. 3,422,921, "Sound Attenuating Wall for Blocking Transmission of Intelligible Speech" (1969).
[3] C. I. Holmer, "The Coincidence Wall, A New Design for High Transmission Loss or High Structural Damping," paper presented at 77th Meeting of the Acoustical Society, April 1969, Sec. K4.
[4] D. Ross, E. Ungar, and E. Kerwin, "Damping of Plate Flexural Vibrations by Means of Viscoelastic Laminae," *Structural Damping*, Sec. III, edited by J. E. Ruzicka (ASME, New York, 1959).
[5] J. E. Manning, "Development of the Coincidence Wall as a High TL Panel," Cambridge Collaborative Report No. 1, 1971.
[6] R. D. Lord, P. Ford, and A. W. Walker, "Sound Transmission Through Sandwich Constructions," J. Sound Vib. **5**, 9–21 (1966).
[7] C. Smolenski and E. Krokosky, "Dilatational-Mode Sound Transmission in Sandwich Panels," paper presented at 76th Meeting of the Acoustical Society of America, November 1968.
[8] C. L. Dym and M. A. Lang, "Transmission of Sound Through Sandwich Panels," J. Acoust. Soc. Am. **56**, 1523–1532 (1974).
[9] J. A. Moore, "Sound Transmission Loss Characteristics of Three Layer Composite Wall Constructions," Ph.D. thesis, Massachusetts Institute of Technology, 1975.

[10] C. L. Dym and D. C. Lang, "Transmission Loss of Damped Asymmetric Sandwich Panels with Orthotropic Cores," J. Sound Vib. **88**, 299–319 (1983).
[11] S. E. Makris, C. L. Dym, and J. M. Smith, "Transmission Loss Optimization in Acoustic Sandwich Panels," J. Acoust. Soc. Am. **79**, 1833–1843 (1986).
[12] J. A. Moore and R. H. Lyon, "Mode Canceling Composite Panel for Greater than Mass-Law Transmission Loss in the Principal Speech Bands," US Patent No. 4,106,588 (August 1978).
[13] I. Ver and C. Holmer, "Interaction of Sound Waves with Solid Structures," in *Noise and Vibration Control*, edited by L. Beranek (McGraw-Hill, New York, 1971), Chap. 11.
[14] A. Ordubadi and R. H. Lyon, "Effect of Orthotropy on the Sound Transmission through Plywood Panels," J. Acoust. Soc. Am. **65**, 133–139 (1979).
[15] Y. Stavsky and N. J. Hoff, "Mechanics of Composite Structures," in *Composite Engineering Laminates*, edited by A. Dietz (MIT, Cambridge, MA, 1969), Chap. 1.